Preprints, 4th IFAC Conference on
Advances in Proportional-Integral-Derivative Control
Almería, Spain | June 12-14, 2024

Overactuation for Active Damping in Compliant Positioning Stage using Piezoelectric Transducers

A.M. Natu * **M.B. Kaczmarek** * **S.H. HosseinNia** *

* *Department of Precision and Microsystems Engineering, Delft University of Technology, Mekelweg 2, 2628 CD Delft, The Netherlands (a.m.natu@tudelft.nl; m.b.kaczmarek@tudelft.nl; s.h.hosseinniakani@tudelft.nl)*

Abstract: In non-collocated compliant positioning systems, the parasitic resonance peak induces undesirable vibrations, limiting control bandwidth. Despite conventional notch filters being employed alongside PID controllers for improving bandwidth, parasitic resonance effects persist in disturbance rejection. This paper introduces an overactuation-based solution, utilizing additional actuators for active damping control to enhance closed-loop disturbance rejection within a PID-based control architecture. Integrating distributed piezoelectric bender actuator-sensor pairs in a collocated configuration further improves damping. A formulated mathematical framework substantiates the benefits, validated by an experimental setup serving as a proof of concept. The proposed solution effectively suppresses parasitic resonance, enhances end-effector disturbance rejection, and achieves higher control bandwidth in the positioning system.

Keywords: Overactuation, Active Damping Control, PID, Positive Position Feedback, Piezoelectric Transducers, Positioning Stage, Distributed Actuators

1. INTRODUCTION

The ever-increasing demands for high throughput and positioning accuracy, driven by accelerating technological advancements in nano-science, have led to extensive utilization of positioning systems with flexure-based mechanisms in the high-tech industry. These systems find applications in various fields, including wafer alignments (Ryu et al. (1997)), scanning probe microscopes (Devasia et al. (2007)), micromanipulators (Lu et al. (2004)), etc. Flexures offer the necessary range of motion while eliminating undesirable friction and backlash. However, their low damping characteristics lead to lightly damped parasitic vibration modes in lightweight and flexible systems at relatively low frequencies, introducing unwanted vibrations that compromise motion performance and accuracy. The typical minimum phase behavior due to non-collocated dynamics and a small damping ratio limits the control bandwidth to a small fraction of the parasitic resonance frequency (Gu et al. (2014)).

Techniques like feedforward, inversion, and notch filters (Steinbuch and Norg (1998)) are combined with conventional PID controllers to mitigate parasitic vibration modes. However, their effectiveness is hindered by uncertainties in system parameters and external disturbances. Feedback controllers, such as integral resonant control (IRC) (Aphale et al. (2007)), integral force feedback (IFF) (Fleming and Leang (2010)), positive position feedback (PPF) (Li et al. (2015)), positive velocity and position feedback (PVPF) (Bhikkaji et al. (2007)), and positive acceleration, velocity, and position feedback (PAVPF) (Li et al. (2017)), are explored as an alternative for damping parasitic resonance modes and enhancing robustness to system uncertainties. PVPF and PAVPF controllers have shown effective damping when appropriately tuned, but their sensitivity to noise, especially in systems equipped with position sensors, poses challenges due to numerical differentiation. The PPF controller exhibits increased robustness with higher controller damping values and second-order high-frequency roll-off characteristics and is frequently combined with collocated piezoelectric bender transducers to provide active damping, where the collocated configuration ensures pole-zero interlacing and enables effective operation of the PPF controller (Preumont (2018)).

In conventional single-axis positioning systems, a Single-Input Single-Output (SISO) configuration is typically employed, utilizing a single actuator and sensor to control. Ideally, the actuator is positioned to facilitate rigid body motion while avoiding the excitation of unwanted parasitic resonances. However, the same actuator is used to suppress undesired resonances and external disturbances through the feedback loop when active damping is required. Furthermore, the attainable maximum damping performance is restricted by both the stability conditions of the damping feedback controller and the saturation limits of the actuator. This creates a conflict, as positioning the actuator for effective damping of undesired modes may compromise optimal motion-tracking performance, where positioning aims to minimize the excitation of these parasitic modes (Schneiders et al. (2004)). Thus, a trade-off is often necessary for satisfactory tracking and damping performance. To address this limitation, researchers have explored the concept of overactuation, involving more

actuators than the number of rigid body modes to be controlled. This technique establishes additional closed-loop feedback interconnections, offering increased freedom to enhance performance, allowing for improved control over system modes while maintaining a favorable balance between the tracking and damping feedback paths (van Herpen et al. (2014), Schneiders et al. (2003)).

In non-collocated compliant positioning systems, the second resonance peak induces undesirable vibrations and limits control bandwidth. While conventional notch filters enable higher control bandwidth, the effect of this parasitic resonance is still observed in closed-loop disturbance rejection performance. This paper proposes a novel overactuation-based solution to overcome these limitations through active control of flexible dynamical behavior, with the main contributions as follows:

(C1) The use of additional actuators enables the implementation of active damping control to improve closed-loop disturbance rejection performance.

(C2) Integrating multiple distributed piezoelectric bender actuator-sensor pairs in a collocated configuration enhances damping performance.

The paper is structured as follows: Section 2 provides an overview of the experimental setup used. Section 3 presents a mathematical model for evaluating system dynamics, including the extended system configuration and control architecture with additional sensors and actuators. Section 4 mathematically substantiates the paper's contributions and presents the experimental results. Finally, Section 5 summarizes the conclusions drawn from the study.

2. SYSTEM DESCRIPTION

The experimental setup described in this paper is a single-axis dual-stage compliant micro-motion system, as illustrated in Fig.1. The system consists of two stages in a series: a base stage and an end-effector platform. The two stages are connected with a set of four parallel guiding flexures, while another set of parallel flexures connects the base mass to the reference ground. These guiding flexures provide the translation degree of freedom to the stages. The entire setup is placed on a vibration isolation platform.

A race-coil Lorentz actuator is employed to actuate the base stage. The position of the end-effector platform is measured using a laser interferometer (with a resolution of 39.5 nm) and an optical mirror mounted on the end-effector platform. The Lorentz actuator generates a bi-directional force directly proportional to the input current. A current amplifier amplifies and converts input voltage signals into the necessary current levels with a constant gain factor during the amplification process. The desired force output can be achieved by precisely controlling the input current to the Lorentz actuator, enabling precise actuation and control of the system.

For overactuation, additional piezoelectric bender actuator and sensor pairs are bonded to the flexures connecting the base stage and end-effector at locations of maximum strain. This ensures reasonable observability and controllability of the flexure resonance in the collocated channel.

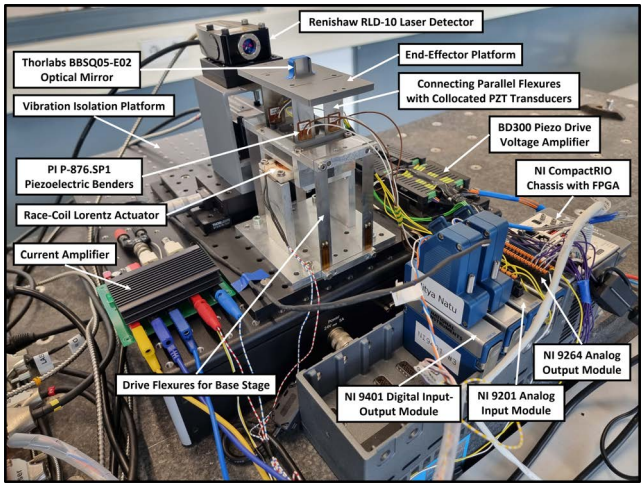

Fig. 1. Experimental Setup

The piezoelectric actuators are driven by voltage signals amplified by a voltage amplifier. An NI CompactRio system with an embedded FPGA facilitates the actuation signals and control. The system includes various analog and digital input-output modules that enable the transmission and reception of signals for implementing the control approach. The control scheme is implemented using NI LabView software, which interfaces the host computer and the micro-motion system.

3. SYSTEM MODELLING AND CONTROL

The system can be analytically analyzed by simplifying it to a double-mass-spring-damper configuration, effectively capturing the behavior of its first two primary modes. Linear behavior is assumed for small displacements of the end-effector platform. Thus, the non-collocated system dynamics, $G(s)$, from the Lorentz actuator force to the position output of the end effector platform ($F_{\text{act}} \mapsto x_2$), is given by the fourth-order transfer function as follows;

$$G(s) = \frac{c_2 s + k_2}{(m_2 s^2 + c_2 s + k_2)[m_1 s^2 + (c_1 + c_2)s + (k_1 + k_2)] - (c_2 s + k_2)^2} \tag{1}$$

Here, m_1 and m_2 represent the mass of the base stage and end-effector platform, while k_1, c_1, and k_2, c_2 represent the total stiffness and damping for the base flexures and connecting flexures respectively.

The combined damping for parallel flexures in the x-direction, c_i, can be expressed as:

$$c_i = 2 \cdot (n_f \cdot \zeta_i) \cdot \sqrt{k_f \cdot m_f} \quad \text{for i} = 1,2 \tag{2}$$

where ζ_i denotes the modal damping of the flexure, and $k_f = k_i/n_f$ and $m_f = m/n_f$ are the stiffness of a single flexure and the effective mass perceived by a single flexure, respectively.

Additionally, the SISO non-collocated plant, denoted as $G(s) = f(c_2)$, is influenced by the parasitic resonance peak height, which is approximately equal to $1/(2\zeta_2)$. According to Eq.1, an increase in the modal damping coefficient of the connecting flexures (ζ_2) corresponds to a decrease in the peak height in the frequency domain. By implementing active damping control, it becomes possible to enhance the system's damping characteristics and effectively reduce the peak height associated with the undesired resonance mode.

3.1 Dynamics of Extended System with Additional Actuators and Sensors

Piezoelectric bender sensors and actuator patches are strategically collocated at locations of maximum strain induced by parasitic resonance on flexures to counteract undesired end-effector platform movement (Moheimani and Fleming (2006)). Transverse displacement $w(x)$ of the flexure, caused by relative displacement $x_d(:= x_2 - x_1)$ between the end-effector platform and base stage, results in strain distribution. This strain induces a small longitudinal patch extension proportional to x_d. The sensor's output charge (Q) is directly proportional to the difference in slopes w' or rotations $\Delta\theta$ at the sensor patch's two extremities (a and b).

$$Q \propto \Delta\theta_i^s \propto [w'(b) - w'(a)] \tag{3}$$

Subsequently, the generated charge across sensor electrodes results in a voltage signal, V_s, which the damping controller processes to produce an actuation voltage, V_a. This voltage drives the piezoelectric actuator to exert equal and opposite forces on masses m_1 and m_2, based on their relative displacement. For simplicity, we exclude base stiffness (k_1) and damping (c_1), modeling connecting parallel flexures as a single equivalent spring (k_2) and damper (c_2). When piezoelectric transducers are collocated in all equivalent flexures, they act as a single sensor-actuator pair, amplifying the output force with increased collocated patches for active damping. In the presented setup, each flexure integrates one pair, allowing a maximum of four active pair patches for control ($0 \leq n \leq 4$).

The extended system configuration is designed by incorporating additional inputs and outputs to accommodate the operation of the piezoelectric transducers. The extended configuration, denoted as G_{ext}, satisfies the following relationship:

$$[\, I \;\; 0 \,]\, G_{\text{ext}}(s) \begin{bmatrix} I \\ 0 \end{bmatrix} = G(s) \tag{4}$$

where $G(s)$ represents the non-collocated dynamics, while $G_{\text{ext}} : [\, F_{\text{act}} \;\; V_a \,]^T \mapsto [\, x_2 \;\; V_s \,]^T$. Here, V_a and V_s are the actuation and sensing signal voltage of the piezoelectric transducers placed in a collocated configuration on each of the flexure.

Accordingly, the state-space equations for this extended equivalent system can be expressed as follows:

$$\begin{Bmatrix} \ddot{x}_1 \\ \ddot{x}_2 \\ \dot{x}_1 \\ \dot{x}_2 \end{Bmatrix} = \begin{bmatrix} -\frac{c_2}{m_1} & \frac{c_2}{m_1} & -\frac{k_2}{m_1} & \frac{k_2}{m_1} \\ \frac{c_2}{m_2} & -\frac{c_2}{m_2} & \frac{k_2}{m_2} & -\frac{k_2}{m_2} \\ 1 & 0 & 0 & 0 \\ 0 & 1 & 0 & 0 \end{bmatrix} \begin{Bmatrix} \dot{x}_1 \\ \dot{x}_2 \\ x_1 \\ x_2 \end{Bmatrix} + \begin{bmatrix} \frac{1}{m_1} & -\frac{n}{m_1} \\ 0 & \frac{n}{m_2} \\ 0 & 0 \\ 0 & 0 \end{bmatrix} \begin{Bmatrix} F_{act} \\ V_a \end{Bmatrix} \tag{5}$$

$$\begin{Bmatrix} x_2 \\ V_s \end{Bmatrix} = \begin{bmatrix} 0 & 0 & 0 & 1 \\ 0 & 0 & p & -p \end{bmatrix} \begin{Bmatrix} \dot{x}_1 \\ \dot{x}_2 \\ x_1 \\ x_2 \end{Bmatrix} + \begin{bmatrix} 0 & 0 \\ 0 & f_d \end{bmatrix} \begin{Bmatrix} F_{act} \\ V_a \end{Bmatrix} \tag{6}$$

Consequently, the input-output relations can be represented as:

$$\begin{Bmatrix} x_2 \\ V_s \end{Bmatrix} = \underbrace{\begin{bmatrix} G_{11} & G_{12} \\ G_{21} & G_{22} \end{bmatrix}}_{G_{\text{ext}}(s)} \begin{Bmatrix} F_{act} \\ V_a \end{Bmatrix} \tag{7}$$

The simplified Multiple-Input Multiple-Output (MIMO) transfer function matrix $G_{\text{ext}}(s)$ is obtained as follows:

$$G_{\text{ext}}(s) = \begin{bmatrix} \frac{c_2 s + k_2}{m_1 m_2 s^2 \left(s^2 + 2\zeta_n \omega_n s + \omega_n^2\right)} & \frac{n}{m_2 \left(s^2 + 2\zeta_n \omega_n s + \omega_n^2\right)} \\ \frac{p}{m_1 \left(s^2 + 2\zeta_n \omega_n s + \omega_n^2\right)} & \frac{-n \cdot p}{m_c \left(s^2 + 2\zeta_n \omega_n s + \omega_n^2\right)} + f_d \end{bmatrix} \tag{8}$$

It should be noted that these equations are simplified by neglecting rigid body dynamics. This simplification allows for the presentation of the system dynamics primarily in the interested frequency range ($\omega > \omega_r$, where ω_r is the rigid body mode frequency), which mainly includes the parasitic resonance mode.

3.2 Control Architecture with Additional Actuators and Sensors

An extended non-collocated system is synthesized by incorporating additional piezoelectric actuator and sensor pairs for active damping control. To illustrate the interactions between motion tracking control and active damping control, a combined control architecture is presented in Fig.2. It consists of two distinct loops: (1) the outer feedback loop utilizing a standard PID controller C_{PID} to achieve accurate motion tracking, and (2) the inner feedback loop employing a PPF controller C_{PPF} to address the damping requirements of the system.

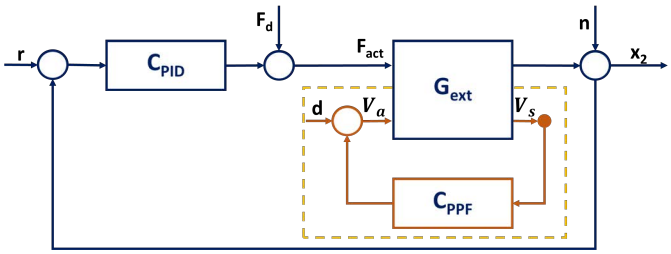

Fig. 2. Control Architecture implementing Active Damping Control

Tamed PID Controller: A conventional tamed Proportional-Integral-Derivative (PID) controller is employed as the motion-tracking controller in the system. The transfer function of linear PID in series form is given by:

$$C_{\text{PID}}(s) = k_p \underbrace{\left(1 + \frac{\omega_i}{s}\right)}_{\text{Integrator}} \underbrace{\left(\frac{s}{\omega_d} + 1\right)}_{\text{Lead}} \underbrace{\left(\frac{s}{\omega_t} + 1\right)^{-1}}_{\text{Lag}} \underbrace{\left(\frac{\omega_l}{s + \omega_l}\right)}_{\text{Low-Pass}} \tag{9}$$

where ω_i is the frequency at which integral action is disabled, ω_l is the cutoff frequency of the low-pass filter (LPF), k_p represents the proportional gain, ω_d indicates the frequency at which differentiating action is initiated, and ω_t represents the frequency at which differentiating action is tamed. Taming prevents high-frequency noise amplification, and the LPF attenuates noise and unmodeled higher-order system dynamics.

To tune the PID controller, with bandwidth frequency ω_c, the following rules of thumb are used (Dastjerdi et al. (2018)):

$$\omega_d = \omega_c/3; \;\; \omega_t = 3\omega_c; \;\; \omega_i = \omega_c/10; \;\; \omega_l \geq 10\omega_c;$$
$$k_p = \frac{1}{3}\left|\frac{1}{G_{11}(i\omega)}\right|_{\omega_c} \tag{10}$$

The controller design requirements aim to maintain stability and robustness by achieving sufficient gain margin (GM $\geq$ 6dB) and phase margin (PM $\geq 30°$).

PPF Controller: The controller operates on the collocated channel, utilizing the voltage signal from the piezoelectric sensor, directly proportional to flexure-induced strain. It processes this input, producing an output voltage signal for the piezoelectric actuator, which actively generates counter-bending moments to suppress undesired vibrations at the target frequency. The controller is represented as a second-order low-pass filter, given as:

$$C_{\text{PPF}} = g_0^{-1}\frac{g\omega_c^2}{s^2 + 2\zeta_c\omega_c s + \omega_c^2} \tag{11}$$

where ω_c is the corner frequency of the controller, ζ_c is the controller damping, g is the controller gain, and g_0^{-1} is the inverse of the steady state gain of the respective collocated channel frequency response.

4. OVERACTUATION FOR FLEXIBLE MODE CONTROL

4.1 Amplifying Damping Performance: The Impact of Additional Distributed Actuators

The damping factor of the closed-loop system by the PPF controller can be expressed in terms of the relationship between the amplitude at resonance and the damping factor (Kwak et al. (2004));

$$\zeta_{i_{CL}} = \zeta_i + \frac{g^2}{4\zeta_c} \tag{12}$$

Thus, in the case of a SISO feedback loop for active damping, the damping ratio experiences an increase. This increase in the damping ratio corresponds to an increase in the damping ratio of a single flexure ($\zeta_{i_{CL}}$) in the described system when the active damping control loop is activated. The maximum increase is observed when the compensator frequency ω_c matches the structure frequency ω, and the maximum unity gain ($g = 1$) is achieved in a stable closed-loop system. As a result, the limitation on the maximum gain for stability constrains the maximum increase in the flexure's damping ratio. This is where overactuation proves advantageous by allowing additional feedback connections to exert a more significant influence on the overall damping ratio of the parallel flexures. When the piezoelectric sensor-actuator pairs are bonded to each flexure, a MIMO system is established, involving n possible active damping feedback loops. Utilizing Eq.(2) and Eq.(12), it can be demonstrated that the total damping coefficient of the parallel flexures in the closed loop is given by:

$$\zeta_{CL} = n_f \cdot \zeta_i + \underbrace{n \cdot \frac{g^2}{4\zeta_c}}_{\substack{\text{Increased} \\ \text{Damping Ratio}}} \tag{13}$$

To illustrate the effects of overactuation through experimentation, an inner feedback loop incorporating a feedback controller is utilized to mitigate the inherent characteristics of the open-loop plant. The damping performance is investigated as the number of active piezoelectric actuator-sensor patch pairs (n) varies.

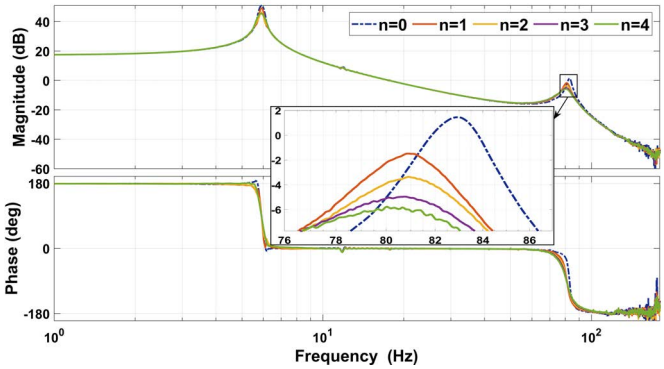

Fig. 3. Impact of Number of Active Piezoelectric Patches on Damping Magnitude in Performance Channel Observed Experimentally

In the context of the system studied in this paper, the parameter n varies within the $0 < n < 4$ range. The outcomes validate that activating additional feedback connections results in an intensified damping effect on the parasitic resonance mode. Notably, when all loops are active, a substantial reduction of 7.2 dB is observed in the peak magnitude within the frequency domain, as depicted in Fig.3. Tuning the damping controller at a frequency higher than the resonance frequency results in a slight decrease in stiffness, evident by a slightly lower closed-loop resonance frequency.

To gain a more comprehensive understanding of the system's response to disturbances, an analysis in the time domain is conducted by applying a disturbance signal with a frequency of 82Hz, corresponding to the parasitic resonance frequency, to the outer open-loop system, and the resultant position output is measured. Consistent with the earlier findings, it is apparent from Fig.4 that activating more feedback loops leads to a decrease in the magnitude of fluctuations in the output position.

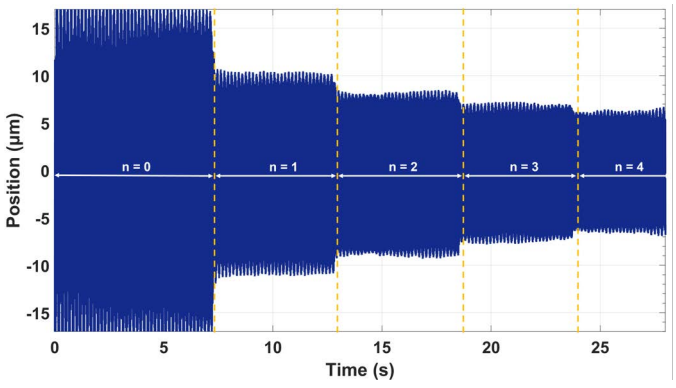

Fig. 4. Experimental Illustration of Impact of Number of Active Piezoelectric Patches on Position Accuracy in Time Domain

4.2 Exploiting Overactuation: Enhancing Disturbance Rejection with Active Damping Control

To demonstrate the advantages of implementing active damping control with additional actuators on the closed-loop disturbance rejection performance, a comparison is made with a standard control architecture using a conventional notch filter (N), as depicted in Fig.5. The evaluation of this performance involves comparing the closed-loop process sensitivity function ($F_d \mapsto x_2$).

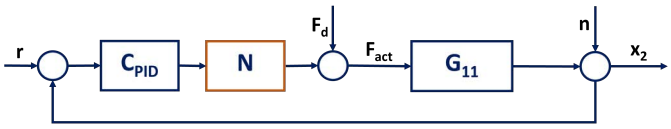

Fig. 5. Control Architecture implementing Notch Filter

Case 1: Closed-Loop Process Sensitivity implementing Active Damping Control: In the inner closed-loop for active damping control with the damping controller C_{PPF}, depicted in Fig.2, the damped system G_d from actuator force F_{act} to position output x_2 is given as:

$$\frac{x_2}{F_{act}} = G_{11} - G_{12} \cdot \frac{C_{\text{PPF}}}{1 + G_{22} \cdot C_{\text{PPF}}} \cdot G_{21}$$
$$G_d = G_{11} \underbrace{\left(1 - \frac{1}{G_{11}} \cdot G_{12} \cdot \frac{C_{\text{PPF}}}{1 + G_{22} \cdot C_{\text{PPF}}} \cdot G_{21}\right)}_{T} \quad (14)$$

The closed-loop process sensitivity implementing active damping control, PS_{ADC} can be computed as:

$$PS_{\text{ADC}} = \frac{G_d}{1 + G_d \cdot C_{\text{PID}}} \quad (15)$$

where G_{11} represents the open-loop non-collocated performance channel dynamics ($F_{\text{act}} \mapsto x_2$).

Case 2: Closed-Loop Process Sensitivity implementing Notch Filter: In this case, the closed-loop process sensitivity implementing notch filter (N), PS_{N} is computed as:

$$PS_{\text{N}} = \frac{G_{11}}{1 + G_{11} \cdot C_{\text{PID}} \cdot N} \quad (16)$$

In practice, the damping controller and the notch filter can be independently tuned to achieve a comparable suppression of the parasitic resonance mode in the open loop (i.e., $G_d = G_{11} \cdot N$). Consequently, the denominators of closed-loop Eq.(15) and Eq.(16) at the parasitic resonance mode frequency will be equal. Therefore, the ratio of the closed-loop process sensitivity in both cases can be expressed as follows:

$$\left|\frac{PS_{\text{ADC}}}{PS_{\text{N}}}\right|_{\omega=\omega_n} = \left|\frac{G_d}{G_{11}}\right|_{\omega=\omega_n} = T < 1 \quad (17)$$

Thus, Eq.(17) demonstrates that when active damping control is employed using overactuation, the magnitude of the closed-loop process sensitivity is reduced around the parasitic resonance frequency, indicating better disturbance rejection performance in the presence of external disturbances, which is not achieved when using a notch filter.

To assess the performance of the closed-loop system, the outer motion tracking loop is closed by implementing a PID controller based on the tuning rules presented in Eq.(10). The controllers are implemented in real-time by discretizing the continuous-time controller using the bi-linear transformation-based Tustin method.

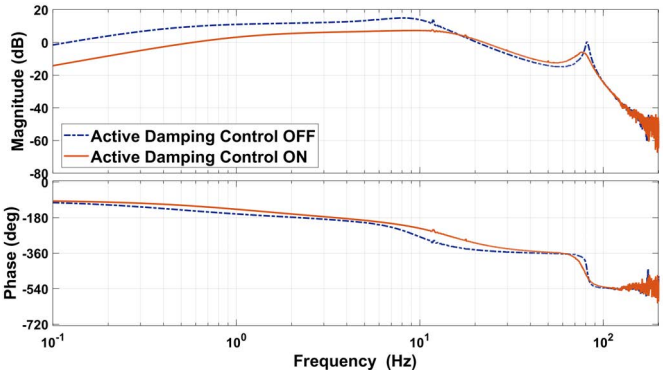

Fig. 6. Closed-Loop Experimental Process Sensitivity Frequency Response

To analyze the improvement in the disturbance rejection performance through the use of damping control for the parasitic flexible dynamics, the frequency response of the closed-loop process sensitivity is measured in two cases: without active damping control and with damping control, where all inner-feedback loops are active (n=4). As depicted in Fig.6, the peak height of the resonance is suppressed by approximately 6.5 dB, indicating a significant improvement in the system's ability to reject disturbances caused by external forces and an enhanced position accuracy of the end-effector platform.

4.3 Controller Tuning for Active Damping

The PPF controller employed for active damping involves three main parameters that require tuning: the controller gain g, the tuning frequency ω_c, and the controller damping ζ_c. A damping factor of 0.3 is selected based on the literature, offering a relatively wide controlled frequency range while maintaining satisfactory performance. To tune the remaining two parameters, a cost function is formulated, considering the reduction in the magnitude of the parasitic resonance peak in the inner closed-loop system $G_d(s)$ and the phase lag introduced in the performance channel $F_{act} \mapsto x_2$ around the desired frequency. Additionally, the cost function incorporates stability constraints ($g < 1$) and no-performance constraints ($g > 0$) through the use of the Kreisselmeier-Steinhauser (KS) function to penalize the constraint violation. Different weights are assigned to each objective, resulting in a weighted multi-objective function J, expressed as:

$$\begin{aligned} J = \; & w_0 \cdot \underbrace{|G_d(iw_n)|}_{\text{Peak Magnitude}} \\ & + \sum_{j=1}^{2} w_j \cdot \underbrace{|\angle G_d(i\alpha_j w_n) - \angle G(i\alpha_j w_n)|}_{\text{Phase Lag due to Active Damping}} \\ & + w_3 \cdot \underbrace{\frac{1}{P} \ln \sum_{k=1}^{2} e^{P \cdot g_k}}_{\text{Penalized Constraints}} \end{aligned} \quad (18)$$

In the provided equation, w_0, w_1, w_2 and w_3 represent the assigned weights, and P denotes the penalty cost.

The constraints are denoted by g_k, while $\alpha_1 = 0.97$ and $\alpha_2 = 1.03$ are factors used to calculate the phase around the natural frequency.

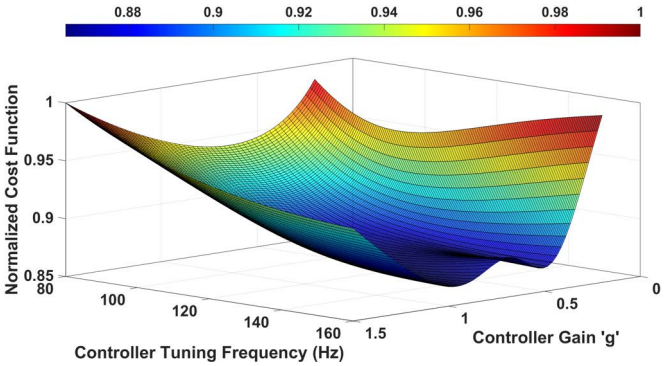

Fig. 7. Parameter Sweep for PPF Controller Tuning

Utilizing the defined cost function, a parameter sweep investigates the influence of controller tuning frequency (ω_c) and gain (g) on the cost function. Fig.7 illustrates the normalized cost function, based on which a controller gain of 0.7 and a targeted frequency of 120 Hz were selected.

5. CONCLUSIONS

The presented research introduces a novel overactuation-based strategy to enhance compliant positioning stages' disturbance rejection performance. The method involves utilizing lightweight piezoelectric actuator-sensor patches strategically bonded to flexures in a collocated configuration at locations of maximum strain to enable overactuation. By implementing active damping control through additional distributed piezoelectric transducers in a collocated configuration, the proposed method effectively dampens parasitic vibrations and external disturbances that affect the position accuracy of the end-effector, overcoming the limitations of traditional notch filters. Increasing the number of active actuators enhances the damping performance, resulting in greater suppression of the targeted resonance peak. The proposed strategy also allows for a higher control bandwidth by mitigating flexible dynamics. A mathematical framework was formulated to generalize the contributions of this work, which were then verified experimentally by using a dual-stage compliant positioning system as a proof-of-concept experimental setup.

The proposed strategy can be further extended to suppress multiple higher-order parasitic modes in flexible systems. While strategic tuning of PPF controllers offers a degree of robustness, performing a detailed robustness analysis in the presence of system uncertainties is further recommended. The scalability and adaptability of overactuated systems, alongside optimizing actuator-sensor configurations, also present exciting prospects for further advancements in positioning system technology.

REFERENCES

Aphale, S.S., Fleming, A.J., and Moheimani, S.R. (2007). Integral resonant control of collocated smart structures. *Smart materials and structures*, 16(2), 439.

Bhikkaji, B., Ratnam, M., and Moheimani, S.R. (2007). Pvpf control of piezoelectric tube scanners. *Sensors and Actuators A: Physical*, 135(2), 700–712.

Dastjerdi, A.A., Saikumar, N., and HosseinNia, S.H. (2018). Tuning guidelines for fractional order pid controllers: Rules of thumb. *Mechatronics*, 56, 26–36.

Devasia, S., Eleftheriou, E., and Moheimani, S.R. (2007). A survey of control issues in nanopositioning. *IEEE Transactions on Control Systems Technology*, 15(5), 802–823.

Fleming, A.J. and Leang, K.K. (2010). Integrated strain and force feedback for high-performance control of piezoelectric actuators. *Sensors and Actuators A: Physical*, 161(1-2), 256–265.

Gu, G.Y., Zhu, L.M., Su, C.Y., Ding, H., and Fatikow, S. (2014). Modeling and control of piezo-actuated nanopositioning stages: A survey. *IEEE Transactions on Automation Science and Engineering*, 13(1), 313–332.

Kwak, M.K., Han, S.B., and Heo, S. (2004). The stability conditions, performance and design methodology for the positive position feedback controller. *Transactions of the Korean Society for Noise and Vibration Engineering*, 14(3), 208–213.

Li, C.X., Gu, G.Y., Yang, M.J., and Zhu, L.M. (2015). Positive position feedback based high-speed tracking control of piezo-actuated nanopositioning stages. In *Intelligent Robotics and Applications: 8th International Conference, ICIRA 2015, Portsmouth, UK, August 24-27, 2015, Proceedings, Part II 8*, 689–700. Springer.

Li, L., Li, C.X., Gu, G., and Zhu, L.M. (2017). Positive acceleration, velocity and position feedback based damping control approach for piezo-actuated nanopositioning stages. *Mechatronics*, 47, 97–104.

Lu, T.F., Handley, D.C., Kuan Yong, Y., and Eales, C. (2004). A three-dof compliant micromotion stage with flexure hinges. *Industrial Robot: An International Journal*, 31(4), 355–361.

Moheimani, S.R. and Fleming, A.J. (2006). *Piezoelectric transducers for vibration control and damping*. Springer Science & Business Media.

Preumont, A. (2018). *Vibration control of active structures: an introduction*, volume 246. Springer.

Ryu, J.W., Gweon, D.G., and Moon, K.S. (1997). Optimal design of a flexure hinge based xyφ wafer stage. *Precision engineering*, 21(1), 18–28.

Schneiders, M.G., Van De Molengraft, M., and Steinbuch, M. (2003). Introduction to an integrated design for motion systems using over-actuation. In *2003 European Control Conference (ECC)*, 3249–3254. IEEE.

Schneiders, M., Van De Molengraft, M., and Steinbuch, M. (2004). Benefits of over-actuation in motion systems. In *Proceedings of the 2004 American control conference*, volume 1, 505–510. IEEE.

Steinbuch, M. and Norg, M.L. (1998). Advanced motion control: An industrial perspective. *European Journal of Control*, 4(4), 278–293.

van Herpen, R., Oomen, T., Kikken, E., van de Wal, M., Aangenent, W., and Steinbuch, M. (2014). Exploiting additional actuators and sensors for nano-positioning robust motion control. *Mechatronics*, 24(6), 619–631.